Computation of tunneling rates in time-dependent electric fields: Electrons on the surface of liquid helium, a one-dimensional hydrogen atom

Gordon F. Saville and John M. Goodkind
University of California, San Diego, La Jolla, California 92093
(Received 7 February 1994)

We have solved, by numerical methods, the time-dependent Schrödinger equation for the known potential of electrons over the surface of liquid helium. The computed tunneling rates for a static field agreed with experimental measurements of the rates. We describe here the extension of the computation to time-dependent electric fields. The results provide quantitative details of the amplitude and frequency dependence of the tunneling rates. They show very large photoassisted enhancements of the tunneling rates. In addition, we find a modulation of the tunneling rates at the frequency of the applied field. The modulation amplitude decreases sharply at frequencies that are integer fractions of the frequency corresponding to the energy difference between the electron ground state and the top of the barrier. We find no evidence of finite transit-time effects.

PACS number(s): 03.65.Ge, 73.40.Gk

I. INTRODUCTION

In previous work [1,2], we have shown that electrons escaping from their shallow potential well, on the surface of liquid helium, are accurately described by a modified [3] one-dimensional (1D) hydrogen atom potential. We did so by comparing a numerical solution of the 1D Schrödinger equation, with this potential, for the tunneling of electrons from the surface of liquid He to tunneling rates measured experimentally. With no adjustable parameters, we found good agreement between experiment and theory over a wide range of applied electric fields and electron density.

The cleanliness of the physical system and the accuracy and simplicity of the algorithm provide an opportunity to investigate fundamental questions about tunneling and the interface between classical and quantum physics. We examine here the response of the system to time-dependent electric fields. Although there is evidence that these tunneling rates are substantially increased by microwave radiation [2,4], no quantitative measurements of the effect have been made. In anticipation of such measurements, we have computed the response to time variations spanning the range between the sudden and adiabatic limits. In the response to periodic variations of the field, we find that photoassisted tunneling becomes important at frequencies approaching the ionization frequency. In that case, tunneling rates can be enhanced by factors as large as 10^8 for modulations of as little as 10^{-3} of the static electric field. We have searched for evidence of the influence of a finite tunneling time or "transit time" through the frequency dependence of the tunneling rate. None has been found. A search for possible influence of classical chaos in this tunneling system is not yet completed.

II. COMPUTATION OF TUNNELING RATES

A simple and frequently used method for estimating tunneling rates uses the WKB approximation. However, the accuracy of the measurements in the case of interest here exceeds the accuracy to which the prefactor to the exponential is determined by this method. More detailed methods that have been used include complex scaling and asymptotic wave functions [4,5]. In our case we require absolute accuracy for the static field case and we compute tunneling in time-dependent potentials where the WKB method cannot be used. We compute both the short-term transient response to sudden changes in the potential as well as the steady-state response to periodic variations. For this purpose, we exploit the fact that the problem is one dimensional to allow us to solve the time-dependent Schrödinger equation numerically with modest computer power. In this approach, no approximations are required other than the necessary representation of the equation in the form of finite differences. The influence of the size of the differences on the solution is readily tested to limit errors to a desired level. No adjustable parameters are introduced into the computation.

Previous computations for this problem by other workers [4] used a combination of analytical and numerical techniques to determine the wave function at large distances from the well, the quasienergies of the states, and the lifetimes (tunneling rates) of the states. Those authors found many of the qualitative features that we describe here. However, in our work, the computation is entirely numerical and much simpler so that a personal computer or workstation can perform the computations rapidly. This has allowed us to explore details of the problem that were not accessible by the earlier methods.

III. THE NUMERICAL ALGORITHM AND TECHNIQUES

The computational algorithm that we use was originally published by Goldberg, Schey, and Schwartz [6,7] and used to generate computer movies of a 1D wave packet scattering off a square barrier. It was later extended to more general 2D scattering problems [8].

The algorithm works by transforming the one-

dimensional time-dependent Schrödinger equation into an implicit, stable, and unitary difference equation. For the implicit scheme to work, boundary conditions must be imposed such that the wave function is zero at the spatial end points of the computation. This is equivalent to placing infinite potential barriers at both of the end points. In the present case the problem is not severe at the liquid-helium surface since the barrier to penetration into the liquid is very high. However, in the vacuum space above the liquid, the portion of the wave function which has tunneled out of the well will eventually reflect back from the far barrier and interfere with subsequent tunneling.

We have used two different methods to circumvent this problem. The first placed the upper end point of the spatial grid sufficiently far above the surface so that a steady-state tunneling rate was established before the reflected wave reached the barrier. The second method introduced a smoothly varying, negative pure imaginary potential $V_{\rm Im}$ starting outside the outer classical turning point z_2. This attenuates the portion of the wave function which escapes such that any reflection from the far boundary is negligible. Reflections from $V_{\rm Im}$ itself are negligible so long as it is sufficiently small and smooth. In that case, we find that the calculated rate is insensitive to the exact form of $V_{\rm Im}$. The computed rates for the two methods agree to within a fraction of a percent. Since it is possible to use a much smaller spatial grid when reflections are eliminated, the second method was used for all computations described here.

Figure 1 illustrates the potential, the basic geometry, and the technique followed in calculating the tunneling rate. The full potential of an electron above the surface of the liquid is

$$V(z)=V_D(z)+eEz+V_C(z)\ . \tag{1}$$

V_D is the hydrogenic part arising from the dielectric image potential in the liquid helium. It has the form

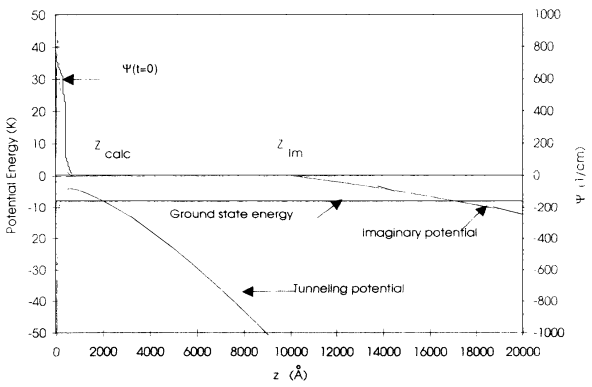

FIG. 1. Geometry of the time-dependent Schrödinger equation alogrithm for static electric fields. In this case $E_{\rm dc}=-26$ V/cm and the density is $n=0.6\times10^7$ cm^{-2}. Although the ground-state energy does not enter into the calculation (it is the initial wave function that is significant), it is also shown in order to show the barrier.

$$V_D(z)=\begin{cases}-\dfrac{\kappa-1}{4(\kappa+1)}\dfrac{e^2}{z+\beta}\ , & z>0\\ +V_0\ , & z<0\ ,\end{cases} \tag{2}$$

where κ is the dielectric constant of liquid helium. The added term β ($\beta=1.04$ Å) in the denominator accounts for the finite distance over which the liquid-helium density changes at the surface. The value we use for it was previously determined by measurement of the microwave absorption spectrum of the bound states [3]. V_0 is the barrier to penetration of an electron into the liquid [9] (≈1 eV). The second term of Eq. (1) is that of the externally applied electric field E. The third term V_C is the electric field due to the other electrons on the surface. The electron densities n that we have studied are not far from those at which the electrons form a two-dimensional crystal so that locally, they are close to that crystalline order. In this range of densities, we have shown [1] that $V_C(z)$ is well represented by a static potential obtained from the Ewald sum [10] over neighboring lattice sites. The vertical component of this electric field $E_z(z)$ varies continuously from zero at $z=0$ (where all the other electrons are in the plane and thus contribute no vertical component) to $E_C=-2\pi ne$ for $z\gg n^{-1/2}$ (the effect of the correlations washes out for heights much greater than typical electron gas nearest-neighbor distances). It is the last two terms of Eq. (1) that decrease the potential at large distances and thus create a wide barrier (≈2000 Å) through which electrons can tunnel.

The electron is typically started, at $t=0$, in the ground state $\psi_0(z)$ of the potential with $E=0$ and $n=0$ and allowed to evolve in time under the influence of the potential with E applied and finite n. This amounts to a sudden application of the electric field to allow tunneling from the ground state of the bound electron. The tunneling potential has inner and outer classical turning points z_1 and z_2, respectively. In a typical case, an imaginary potential of the form

$$V_{\rm Im}(z')=-4.807\times10^{-13}E_{\rm dc}z'\times\exp[0.3z'/(z_{\rm end}-z_{\rm Im})]\ ,\quad z>z_{\rm Im} \tag{3}$$

is introduced at a point $z_{\rm Im}=10\,000$ Å, where $E_{\rm dc}$ is the applied dc electric field in V/cm, $z'=z-z_{\rm Im}$, and $z_{\rm end}$ is the upper boundary of the spatial grid (typically 20 000 Å). The wave function is initially normalized. The escape rate is determined by integrating the probability density from the helium surface to a fixed point $z_{\rm calc}$ (typically $z_{\rm calc}=z_2$) at successive time intervals. With a spatial step size δz and a time step δt, one has

$$F_{\rm in}(t)=\delta z\sum_{n=1}^{n_{\rm max}=z_{\rm calc}/\delta z}\psi_n(t)^*\psi_n(t)\approx\int_0^{z_{\rm calc}}\psi^*(z,t)\psi(z,t)dz \tag{4}$$

and the escape rate is given by

$$W(t)=\frac{F_{\rm in}(t)-F_{\rm in}(t-\delta t)}{\delta t}\ . \tag{5}$$

Suitable step sizes δz and δt were determined empirically by repeating the calculations for a range of values for both. If we use an idealized hydrogenic potential

$$V_D(z)=\begin{cases} -\dfrac{\kappa-1}{4(\kappa+1)}\dfrac{e^2}{z}\ , & z>0 \\ +\infty\ , & z<0 \end{cases} \tag{6}$$

in place of the actual potential of Eq. (2), the results do not depend on the step sizes for $\delta z \leq 2$ Å and $\delta t \leq 2\times 10^{-14}$ sec. However, using the actual potential of Eq. (2), the results are not independent of δz, even for spatial step sizes as small as $\delta z = 0.1$ Å. We describe, in the Appendix, the methods that we used to obtain accurate computations for the actual potential in the static field case.

IV. ESCAPE IN THE PRESENCE OF TIME-DEPENDENT FIELDS

Since there is, at present, no experimental data to compare to in time-dependent electric fields, the idealized hydrogenic potential [Eq. (6)] was used for these calculations so as to allow computation of a large number of cases in a reasonable amount of time.

A. Sudden and adiabatic limits

If the potential is changed very slowly relative to other characteristic times of the problem, a quantum state can adjust adiabatically to the changing potential. In that case, an electron starting in the ground state of the original potential will end up in a corresponding state of the final potential. On the other hand, if the potential is changed very rapidly, an electron originally in the ground state of the initial potential will be in a mixed state of the final potential.

Plots of typical escape rate vs time are shown in Fig. 2. For the "sudden" limit there is an initial surge of very rapid escape, lasting on the order of 2×10^{-10} sec. At the end of the surge there are oscillations in the rate whose details depend on the choice of $z_{\rm calc}$. Similar general features have been seen in an exact solution of escape from a δ potential bound state in the presence of a dc electric field [5]. For the range of experimental fields and densities under consideration, the integrated escape probability in this surge corresponds to approximately 0.1–0.2 %. After approximately 2×10^{-10} sec the escape rate settles down to a constant value, which we define as the tunneling rate. Typically the calculation is carried out to $t=4\times 10^{-10}$ sec. The maximum escape rates we have considered in the dc case are approximately $W=10^3$ sec^{-1}, so that the total escape during the initial transient surge is $\leq 10^{-7}$. The exponential decay of the rate is therefore negligible for these short times.

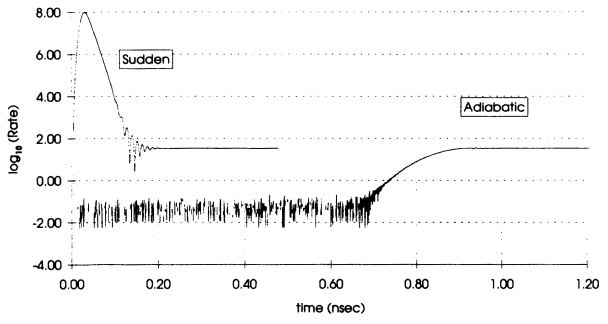

FIG. 2. Comparsion of $W(t)$ in the sudden and adiabatic limits. When the field is turned on slowly enough, there is almost no transient and the rate follows the rate for the instantaneous potential. The scatter around $W(t)=0.1$ sec^{-1} is due to least bit errors.

We have also computed the tunneling rate as a function of time for cases in which the potential was applied gradually according to the following expression:

$$E(t)=\begin{cases} \dfrac{E_{\rm final}}{2}-\dfrac{E_{\rm final}}{2}\cos\left[\pi\dfrac{t}{t_{\rm final}}\right]\ , & t<t_{\rm final} \\ E_{\rm final}\ , & t\geq t_{\rm final}\ , \end{cases} \tag{7}$$

$$E_{\rm final}=-36\ \text{V/cm}\ ,$$

$$t_{\rm final}=9\times 10^{-10}\ \text{sec}\ ,$$

$$n=0\ \text{cm}^{-2}\ .$$

As the field is turned on more slowly, by increasing $t_{\rm final}$, the initial surge of escape becomes smaller (smaller peak rates and smaller total integrated escape in the surge). Figure 2 shows a comparison of the sudden and adiabatic responses for a stripping field of $E_{\rm dc}=-36$ V/cm, $n=0$, and $t_{\rm final}=9\times 10^{-10}$ sec. The only sign of nonadiabaticity is the small oscillations in the rate immediately after the field has reached its final value. The noise at the 0.1-sec^{-1} level is due to the least bit error of the 64-bit calculation. The steady-state tunneling rate is exactly the same for both cases [11].

B. Effect of an applied periodic electric field

Two frequency scales of interest are the inverse of the Büttiker-Landauer [12] time $f_{\rm BL}=1/\tau_{\rm BL}$ (typically on the order of 30 GHz for this problem) and the ionization frequency $f_{\rm ion}=1/hE_{\rm ion}$ of the electron in the well (of order 100 GHz).

Periodic fields also provide a tool for studying the transition to classical chaos [13–15]. For this purpose, a large amount of theoretical and experimental work has been done on the effect of oscillating electric fields on (three-dimensional) hydrogen atoms [16–18]. However, that work has been concerned with ionization in which the electron starts in a high quantum number Rydberg state. Ionization calculations have also been made for a similar semiclassical response of electrons on the surface of liquid helium [19], pointing out that more accurate computations were possible in this case then for the 3D system.

Beyond this question of semiclassical ionization, electrons on helium provide a system in which tunneling and ionization can be explored from the deep quantum regime, in which only one or a few quasibound states exist.

The number of quasibound states is easily varied by changing E_{dc} and n. The Floquet formalism shows that each of these states is coupled to the continuum in the presence of an oscillating field so that complicated paths in phase space are possible. The application of periodic fields has been shown to lead to the suppression of tunneling in the two-well problem [20] and to enhance decay from metastable states [21]. Shaped pulses of light have been used to "guide" chemical reactions [22]. In our case the light pulses would be replaced by pulses of microwave radiation and the computations to be tested by the experiments, described here, involve no approximations.

V. DETAILS OF THE NUMERIC METHOD

In the experimental system, the tunneling barrier can be modulated by adding an oscillating term to the electric field

$$E_{tot}(t)=E_{dc}[1-\alpha_{ac}\sin(2\pi f_{app}t)] , \tag{8}$$

where f_{app} is the applied frequency and α_{ac} is the fractional amplitude of the modulation expressed in terms of E_{dc}. In order to allow rapid computation of a large number of cases, we compute the tunneling with the following parameters. The spatial grid is ended at $z=12\,000$ Å. The annihilating imaginary potential is started close to the outer turning point z_2 and is made steep:

$$\begin{aligned} V_{Im}(z')&=-9.613\times10^{-13}E_{dc}z' \\ &\quad\times\exp[0.6z'/(z_{end}-z_{Im})] , \quad z>z_{Im} , \\ z_{Im}&=z_2+2000 \text{ Å} . \end{aligned} \tag{9}$$

In addition, an analytic approximation for V_C is used. It is obtained from a fit of the potential from the Ewald sum [10] to a model [23] in which the charge density is zero inside a correlation hole of radius R_0 and is a constant n for $\rho\geq R_0$. The constants used for the hydrogenic part of the potential are slightly different from those in the static field case discussed in the Appendix:

$$\begin{aligned} V(z)&=-\Lambda_0\frac{e^2}{z}+eE_{dc}z+V_C(z) , \\ \Lambda_0&=1.606\,76\times10^{-21} , \\ V_C(z)&=-1.451\,61\times10^{-18}n\left[\left[z^2+\frac{0.500\,66}{n}\right]^{1/2}\right. \\ &\quad\left.-\left[\frac{0.500\,66}{n}\right]^{1/2}\right] . \end{aligned} \tag{10}$$

These values result in small changes in the calculated rates relative to those used in the static case where a test of the absolute value of predictions against experiment was the objective. However, the changes are small compared to the effects of using the ideal hydrogenic potential instead of the actual one. Our objective here is to determine the dependence of tunneling rates on the amplitude and frequency of the applied field and these are effected little by these small changes.

In order to reduce the initial transients and to concentrate on the effects of the ac field, we use the quasiground state of the dc tunneling potential as the initial wave function $\psi(t=0)$. It is obtained in one of two ways, either of which is equally efficient at minimizing the initial transients. The first is to use the wave function from the dc problem, after it has run for a long enough time to reach the steady-state tunneling rate. The second is to find the quasiground state directly by numerical means. In either case, the sudden application of the ac field leads to some initial surge of tunneling similar to that caused by suddenly applying the dc field in the static case.

VI. GENERAL CHARACTERISTICS OF THE ESCAPE

We present calculations made in two regimes, corresponding to the upper and lower limits of the tunneling rates observed experimentally in static fields. In the first case, the dc electric field is $E_{dc}=-36$ V/cm and the density is $n=0.5\times10^8$ cm^{-2}. In the second case $E_{dc}=-24$ V/cm and $n=0.0$ cm^{-2}. Frequencies and fractional amplitudes in the ranges $2\leq f_{app}\leq130$ GHz and $0.0001\leq\alpha_{ac}\leq0.1$ have been explored.

For each calculation, information was obtained by computing both the escape rate as a function of time $W(t)$ and the wave function at a position z_{calc} as a function of time $\psi(z_{calc},t)$. Our case differs from most theoretical investigations of time-dependent barriers in that the ac field has a much greater effect on the width of the barrier than on its height.

The presence of an ac component has three general effects on $W(t)$. The first is that the escape rate is higher than in the dc case. The second is that the rate itself is modulated at the applied frequency f_{app}. When the modulation of the tunneling rate is of order 10% or less it is nearly sinusoidal. The third is that the energy of the escaping particle can be modified by the absorption or emission of quanta of energy hf_{app}. In the discussion that follows, this will be referred to as the absorption and emission of photons even though the computation is not explicitly for radiation fields.

Figure 3 shows an example of a case with large nonsinusoidal oscillations. Figure 4 shows details of the sinusoidal oscillations for small modulation. It also shows the sinusoid which is least-squares fit to the steady-state oscillations. The fit function is of the form

$$W_{fit}(t)=W_{av}-W_{osc}\sin(2\pi f_{app}t+\phi_{delay}) , \tag{11}$$

where W_{av}, W_{osc}, and ϕ_{delay} are the fit parameters and correspond to the average dc rate, the amplitude of the ac component, and the phase delay of the ac component relative to the applied ac field, respectively. The phase delay can be interpreted as a delay time $t_{delay}=\phi_{delay}/2\pi f_{app}$ of the wavelets of escaping wave function with respect to the oscillating applied field. The absolute value of t_{delay} is not meaningful as it depends on exactly how "escape" is defined (in these calculations, therefore, on the position of z_{calc}, since a part of the delay time is due to the time for the wavelets to propagate from the outer turning point to z_{calc}). However, changes in the delay time as a function of frequency, for fixed z_{calc}, re-

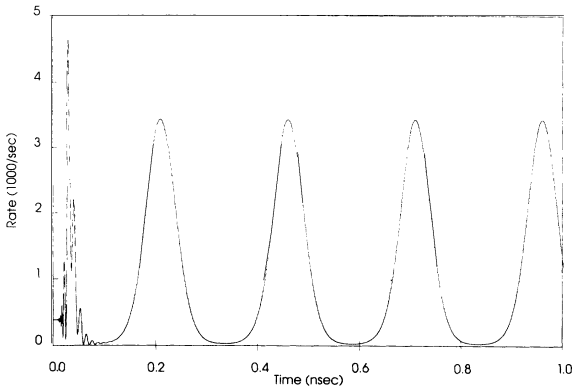

FIG. 3. Example $W(t)$ for applied periodic field (large modulation). Escape rate as a function of time for the case $E_{dc}=-36$ V/cm, $n=0.5\times10^{8}$ cm^{-2}, $f_{app}=4$ GHz, and $\alpha_{ac}=0.10$. After the initial transient due to the sudden application of the ac field, there is a steady nonlinear modulation of the rate at the applied frequency. This type of response is typical when the modulation of the rate is comparable to the rate average.

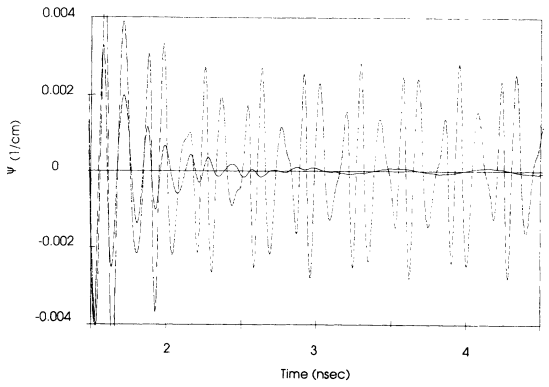

FIG. 5. Multiphoton fit to $\Psi_{Re}(t)$ showing the approach of $\Psi_{Re}(t)$ to its steady-state behavior for times greater than $\sim2\times10^{-10}$ sec. In addition, the residual from a four-photon fit ($n_{max}=4$) of the form of Eq. (12) is shown. The qausi-ground-state energy corresponds to a frequency $f_{GS}=\varepsilon_1/h=-166.2425$ GHz. Thus the five-photon component has a frequency $f_5=f_{GS}+5f_{app}=-16.2425$ GHz, which matches the frequency of the residual when the transient has died away. Thus nearly all of the residual corresponds to a five-photon component.

veal some curious features of the tunneling process.

In order to determine the energies of the escaping electrons we examine $\psi(t)$ at fixed z. Initially there are large oscillations which are the response to the sudden application of the ac field at $t=0$. After $\sim2\times10^{-10}$ sec these oscillations die out and are followed by a much steadier oscillatory pattern which can be decomposed into discrete frequency components. Figure 5 shows $\psi_{Re}(z_{calc},t)\equiv\mathrm{Re}\{\psi(z_{calc},t)\}$ after $t=1.5\times10^{-10}$ sec. It also shows the residual after subtracting a best fit function

$$\psi_{fit}(t)=\sum_{n=-1}^{n_{max}} A_n \sin\left[2\pi\left[\frac{\varepsilon_1}{h}+nf_{app}\right]t+\varphi_n\right] \tag{12}$$

for times after the initial transient has died away, with $n_{max}=4$. The A_n are the fit parameters and represent the amount of the escaping wave function which at $z=z_{calc}$ has an energy corresponding to n photons having been absorbed. Determination of the A_n thus determines the energy content of the escaped electron. However, it is not meaningful to attempt to determine whether the electron is raised to a virtual state inside the well prior to tunneling or whether the quanta are absorbed in the barrier region itself. We show below that some energy is absorbed outside the barrier in the region $z_2\le z\le z_{calc}$.

In summary, the procedure described allows the determination of the average tunneling rate, the amplitude of the modulation of the tunneling rate, the energy spectrum of the escaping electron, and the phase lag (and corresponding time lag) of the escaping wavelets. In the next section we describe the dependence of these quantities on the parameters of the system.

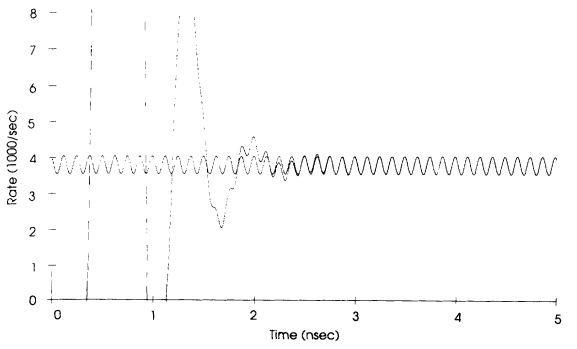

FIG. 4. Sinusoidal fit to $W(t)$ after the transient has died away. The average rate, the amplitude of the oscillations in the rate, and the phase lag between the rate and the applied field are determined from this fit.

VII. RESULTS

A. Single bound state

Figure 6 shows the transition from escape controlled only by the dc field to escape resulting primarily from the oscillatory field. For the low drive level of $\alpha_{ac}=0.0001$ the rate changes very little as a function of frequency from its dc value of $W_{av}=386$ sec^{-1} (the peak average rate is 437 sec^{-1} at a frequency $f_{app}=91$ GHz, about 20% above the ionization frequency of 76.1 GHz). For the case of $\alpha_{ac}=0.02$ there is a clear transition from the dc behavior at frequencies low with respect to f_{ion}, to an escape rate several orders of magnitude greater than the dc rate at frequencies comparable to or greater than f_{ion}. This increase in the rate is due to the electron absorbing one photon and escaping either by direct photoionization at frequencies greater than f_{ion} or by photon-assisted tunneling at frequencies less than f_{ion}. The rate has a photoionization peak at $f_{app}\approx90$ GHz, which is approximately 18% greater than f_{ion}.

Figure 7 shows the breakdown of $\psi_{Re}(z_{calc},t)$ into its

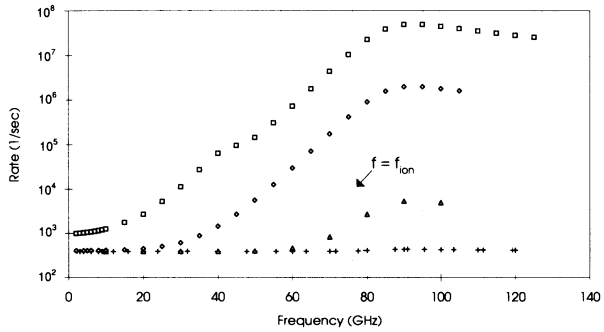

FIG. 6. Average escape vs frequency for case 1, in which $E_{dc}=-36$ V/cm and $n=0.5\times10^{8}$ cm^{-2}. The vertical lines are plotted at $f=(k/4)f_{ion}$, $k=1,2,3,4,5$, and thus show quarter multiples of the ionization frequency. As the level of the modulation of the electric field is increased, the escape due to one photon being absorbed increases. The effect of one-photon absorption is to create a peak in the average rate above the ionization frequency. At $\alpha_{ac}=0.1$ the effect of two-photon absorption can be seen in a small peak at a frequency a little above $f_{ion}/2$. □, $\alpha_{ac}=0.1$; ◇, $\alpha_{ac}=0.02$; △, $\alpha_{ac}=0.001$; +, $\alpha_{ac}=0.0001$.

various energy components, corresponding to different numbers of discrete photons being absorbed as a function of f_{app} for this case. Here also the transition between the dominance of the dc case (no photons being absorbed) at low frequencies to the case at higher frequencies where one-photon absorption is dominant is clear. The one-photon-assisted escape goes through a peak at $f_{app}\approx90$ GHz, corresponding to the peak in the average rate at the same frequency. The case with $\alpha_{ac}=0.001$ is intermediate between the two discussed above, with a transition to one-photon-assisted escape becoming dominant, but at a higher frequency than in the $\alpha_{ac}=0.02$ case.

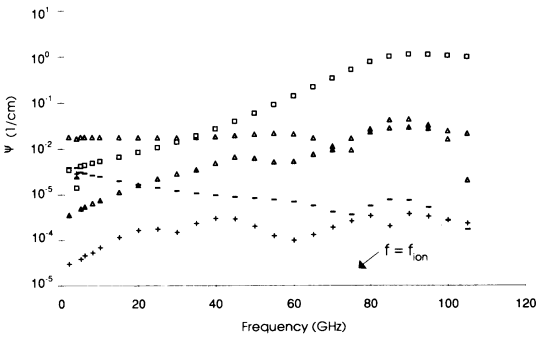

FIG. 7. Breakdown of $\Psi_{Re}(z_{calc},t)$ into its energy components for case 1, in which $E_{dc}=-36$ V/cm, $n=0.5\times10^{8}$, and $\alpha_{ac}=0.02$. This decomposition is determined by a least-squares fit of the form of Eq. (12) to the calculated wave function after the initial transients have died away. Energies corresponding to the emission of one photon to the absorption of three photons are plotted. There is a crossover at a frequency a little below 40 GHz from zero-photon dominance to one-photon dominance. △, zero photons; □, one photon; ▲, two photons; +, three photons; −, minus one photon.

When the modulation is large enough, there is an increase in the rate even when no photons are absorbed, due to the nonlinear dependence of the dc tunneling rate on the applied stripping field. Thus the $\alpha_{ac}=0.1$ curve of Fig. 7 shows a low-frequency average rate of approximately 10^{3} sec^{-1}, which is the average rate for this modulation level when the escape rate adiabatically follows the dc rate of the instantaneous potential. In addition, at this modulation level there is a small peak at a frequency a little greater than one-half the ionization frequency, due to two-photon-assisted escape. Although only a small portion of the wave function in the well should be in this doubly excited state, this portion can escape rapidly due to its higher energy.

Figure 8 shows the average rate as a function of frequency and α_{ac} for $E_{dc}=-24$ and $n=0$. All three drive levels show clear one-photon-assisted escape peaks at 98 GHz, approximately 8% greater than the ionization frequency of 91.1 GHz. In addition, the two larger drive levels show two-photon-assisted peaks at 48 GHz, which is approximately 6% greater than $f_{ion}/2$. As in the previous case, for $\alpha_{ac}=0.10$ the low-frequency limit of the average rate is significantly greater than the dc rate, due to the nonlinear dependence of the dc escape rate on the stripping field. At this drive level there is also an incipient three-photon peak close to $f_{ion}/3$.

Figure 9 is a plot of the photon content of $\psi_{Re}(z_{cal},t)$ as a function of f_{app} for $\alpha_{ac}=0.10$. At frequencies above approximately 60 GHz one-photon-assisted escape is the dominant mechanism. The peak in the one-photon escape occurs at the same frequency as the photoionization peak in the average rate shown in Fig. 8. For frequencies between approximately 40 and 60 GHz the dominant escape mechanism is two-photon-assisted escape. Its peak is also at the frequency of the corresponding peak in the average rate. For frequencies between approximately 20 and 40 GHz the three-photon component is also significant, causing the incipient three-photon peak in the average rate close to $f_{ion}/3$. At very low frequency the escape is adiabatic and thus is no longer limited to the

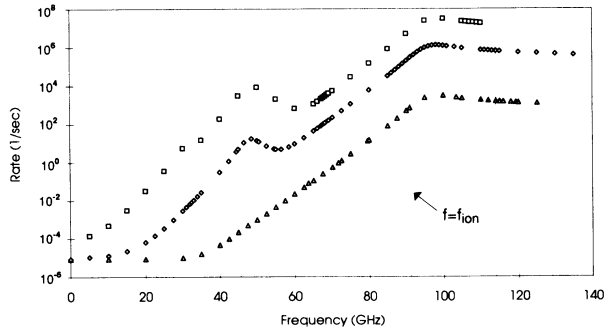

FIG. 8. Average escape vs frequency for $E_{dc}=-24$ V/cm and $n=0.0$ cm^{-2}. The vertical lines are plotted at $f=(k/4)f_{ion}$, $k=1,2,3,4,5$, and thus show quarter multiples of the ionization frequency. Note the clear peaks due to one- and two-photon ionization at frequencies a little above f_{ion} and $f_{ion}/2$ and the incipient three-photon peak in the $\alpha_{ac}=0.1$ curve at $f_{ion}/3$. □, $\alpha_{ac}=0.1$; ◇, $\alpha_{ac}=0.02$; △, $\alpha_{ac}=0.001$.

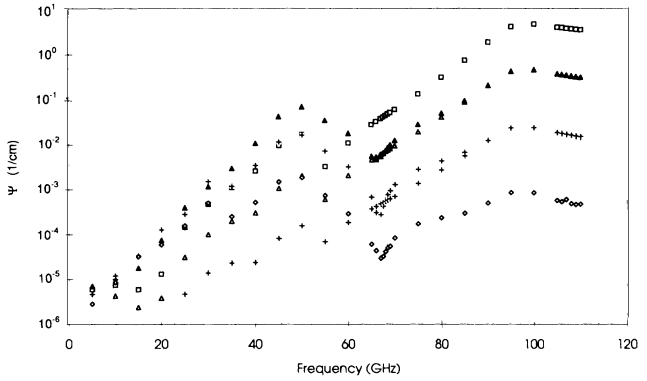

FIG. 9. Breakdown of $\Psi_{\mathrm{Re}}(z_{\mathrm{calc}},t)$ into its energy components for case 2, in which $E_{\mathrm{dc}}=-24$ V/cm, $n=0$ cm^{-2}, and $\alpha_{\mathrm{ac}}=0.10$. This decomposition is determined by a least-squares fit of the form of Eq. (12) to the calculated wave function after the initial transients have died away. Energies corresponding to the absorption of zero to four photons are plotted. Two-photon absorption is dominant at the 50-GHz peak and one-photon absorption is dominant at the 100-GHz photon peak. △, zero photons; □, one photon; ▲, two photons; +, three photons; ◇, four photons.

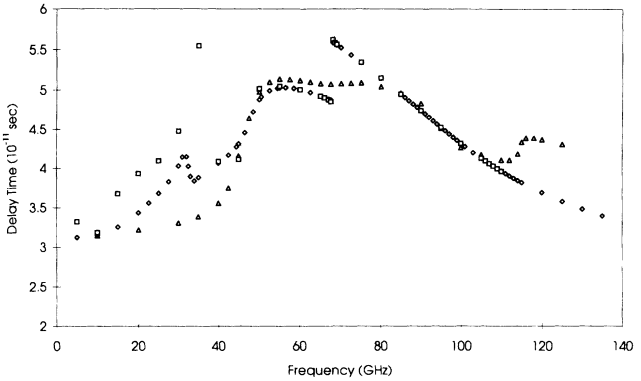

FIG. 11. Delay time τ_{delay} vs frequency for case 2, in which $E_{\mathrm{dc}}=-24$ V/cm and $n=0$ cm^{-2}. There are sudden jumps, corresponding to a phase change of $\pm\pi$, at $f_{\mathrm{app}}=3f_{\mathrm{ion}}/8$, $f_{\mathrm{app}}=3f_{\mathrm{ion}}/4$, and $f_{\mathrm{app}}=5f_{\mathrm{ion}}/4$, depending on α_{ac}. △, $\alpha_{\mathrm{ac}}=0.001$; ◇, $\alpha_{\mathrm{ac}}=0.02$; □, $\alpha_{\mathrm{ac}}=0.10$.

discrete frequencies $f_n=\varepsilon_1/h+nf_{\mathrm{app}}$. Rather the spectrum is a continuum of frequencies corresponding to the range of quasi-ground-state energies of the electron in the well.

Another feature of this case is that the less dominant mechanisms tend to follow the frequency dependence of the dominant mechanism, but at a lower level. We suspect that this is due to stimulated transitions from the portion of the wave function escaping in the dominant mode to states whose energies are different by nhf_{app} (n an integer) after the electron is outside the barrier. Because transitions up and down in energy are equally likely, the amplitudes for the total energy corresponding to zero photons and two photons having been absorbed lie on top of each other at high frequencies (both are separated from the dominant one-photon state by a single photon). Since tunneling rates depend on energy, these amplitudes would not be equal if the transitions were taking place inside of the well.

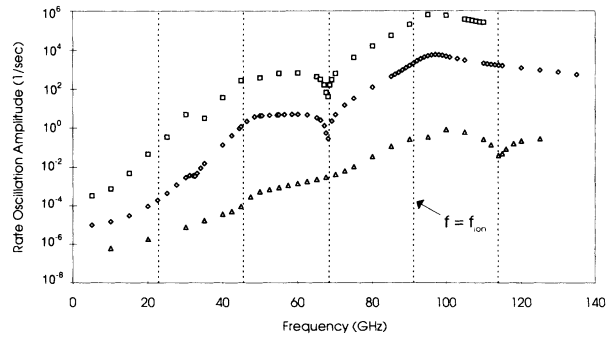

FIG. 10. Rate modulation amplitude vs frequency for case 2 [as determined by the fit to Eq. (11)]. In this case $E_{\mathrm{dc}}=-24$ V/cm and $n=0.0$ cm^{-2}. The vertical lines are plotted at $f=(k/4)f_{\mathrm{ion}}$, $k=1,2,3,4,5$, and thus show quarter multiples of the ionization frequency. There is a sharp decrease in the size of the modulation at $f=0.75f_{\mathrm{ion}}$ for $\alpha=0.02$ and 0.1. For $\alpha_{\mathrm{ac}}=0.001$ the decrease occurs at $f=1.25f_{\mathrm{ion}}$. It also appears that there is an effect at a frequency close to $3f_{\mathrm{ion}}/8$. □, $\alpha_{\mathrm{ac}}=0.1$; ◇, $\alpha_{\mathrm{ac}}=0.02$; △, $\alpha_{\mathrm{ac}}=0.001$.

Figure 10 is a plot of the amplitude of the *modulation* of the escape rate, as a function of f_{app}. Figure 11 shows the delay time $t_{\mathrm{delay}}=\phi_{\mathrm{delay}}/2\pi f_{\mathrm{app}}$ as a function of f_{app} for the same case. The most interesting features are the sharp dips in the amplitude of the oscillations and the corresponding shifts in the phase by $\pm\pi$. For the lowest drive level ($\alpha_{\mathrm{ac}}=0.001$) these features occur at $f_{\mathrm{app}}=5f_{\mathrm{ion}}/4$. For the two higher drive levels ($\alpha_{\mathrm{ac}}=0.02$ and 0.10) they occur at $f_{\mathrm{app}}=3f_{\mathrm{ion}}/4$. In all cases, when the oscillation amplitudes pass through a minimum the remaining small modulation of the rate is primarily at twice the frequency of the applied field. In addition, at the two higher drive levels, there is a large feature in the delay time and a small one in the amplitude of the oscillations close to $f_{\mathrm{app}}=3f_{\mathrm{ion}}/8$.

B. Multiple bound states

The number of quasibound states in this system can easily be changed by varying the applied dc field and/or the electron density. Such additional quasibound states have energies close to the top of the potential barrier (the unperturbed ideal 1D hydrogen potential has energy levels which vary as $\varepsilon_n \propto 1/n^2$). This region is particularly interesting to explore both numerically and experimentally since the region close to the top of the barrier (the classical separatrix) is one of the regions where classically one expects chaos to first appear.

Only a limited examination of the system in a state in

which the dc analog has more than one quasibound state has been made. The only conclusion reached to date is that frequencies corresponding to the differences in energy between the quasibound levels and between the quasibound levels and the continuum are important. One way in which these frequencies manifest themselves is that the escape rate $W(t)$ can no longer be modeled as a dc rate plus an ac component at $f_{\rm app}$.

VIII. CONCLUSIONS

Our study of the single bound state case can be summarized as follows. The energy, and hence time scale, of importance in every case is the ionization frequency $f_{\rm ion}$. No features are observed at the frequency corresponding to the Büttiker-Landauer time $\tau_{\rm BL}$. This includes the peculiar dip in the oscillation amplitude and phase shift at $f_{\rm app}=3f_{\rm ion}/8$ even though this frequency is close to $1/\tau_{\rm BL}$.

For the relatively low drive levels examined thus far, there have been no manifestations of chaos. The average escape rate itself can be explained by photon-assisted tunneling or photoionization at high frequencies and by adiabatic behavior at low frequencies and large drive amplitude. One-, two-, and three-photon-assisted escape peaks have been observed at frequencies corresponding to $f_{\rm ion}, f_{\rm ion}/2$, and $f_{\rm ion}/3$, respectively.

The computations have revealed a new feature of the tunneling process which is a modulation of the tunneling rate at the frequency of the applied field. Particularly at the higher drive levels there is structure in the amplitude and phase of this modulation. These features are also related to the ionization frequency and have occurred at $3f_{\rm ion}/8$, $3f_{\rm ion}/4$, and $5f_{\rm ion}/4$. They are apparently due to wave interference, but we have not yet explained it in detail. Although we know of no method to observe this modulation directly, its possible influence on the radiation field and thus on the impedance of a microwave cavity is being examined.

ACKNOWLEDGMENTS

The authors gratefully acknowledge helpful conversations with Kim Greist, Martin Holthaus, and Peter Hänggi. This work was supported by the National Science Foundation under Grant No. DMR 88-19507.

APPENDIX: ACCURATE COMPUTATIONS FOR A STATIC ELECTRIC FIELD

In order to obtain results valid for the limit $\delta z \to 0$, several lengthy calculations are required for each case. However, an alternative described below was used that avoided the need to repeat this computation for each case. The ground-state energy for the actual potential (2) differs from that of the idealized 1D hydrogen potential (6) by about 5%. This makes a very substantial difference in the tunneling rates so that the actual potential must be used to obtain sufficient accuracy to compare to the experimental results.

Since the tunneling rate is calculated by taking the difference between two nearly equal numbers, for rates $\leq 0.5\ \sec^{-1}$ the least bit error in the difference becomes significant for 64-bit calculations. To resolve this problem, for rates less than approximately $1\ \sec^{-1}$, 128-bit precision is used in the calculations.

In order to minimize the amount of computing time required to solve the Schrödinger equation for the actual potential of Eq. (2), most of the comparisons to experiment in the static potential were made indirectly by first comparing the WKB results to the exact solution of the Schrödinger equation for the case in which the hydrogenic part to the potential of Eq. (1) is given by the ideal case of Eq. (6).

The WKB rate is computed from the usual expression

$$W = C_{\rm cal}\frac{\varepsilon_1}{\hbar}\exp\left[-\frac{2}{\hbar}\int_{z_1}^{z_2}\sqrt{2m[V(z)-\varepsilon_1]}\,dz\right] \tag{A1}$$

using the conventional prefactor of $\varepsilon_1/\hbar$, where ε_1 is the Stark shifted ground-state energy, $C_{\rm cal}=1.38$ is the "calibration" factor determined by comparison to the exact numerical solutions for the idealized potential. In this case the ground-state energy is

$$\varepsilon_1 = -7.6368 + 0.013\,24[E_{\rm dc}({\rm V/cm})]\ {\rm K}\ . \tag{A2}$$

Since $\{2m[V(z)-\varepsilon_1]\}^{1/2}$ is slowly varying inside the barrier except near the classical turning points, we expected that the WKB approximation would yield valid field and density dependencies for the rate. In practice the WKB tunneling rates, using the calibration factor, agree [2] with the exact computation to within 7% for rates between 10^{-5} and $10^{3}\ \sec^{-1}$. In order to make comparisons to the experimental data (in static fields) the WKB rate was then calculated for the actual 1D potential [Eq. (2)] by using the Rydberg energy and Stark shift computed for this potential

$$\varepsilon_1 = -8.01 + 0.012\,55[E_{\rm dc}({\rm V/cm})]\ {\rm K} \tag{A3}$$

and using $C_{\rm cal}=1.38$.

For the range of electric fields used in the experiment, all the excited bound states for the idealized hydrogenic potential move into the continuum in the presence of the stripping field. The only quasibound state remaining is the one corresponding to the ground state in the absence of the field. If we use the wave function for this ground state as the initial state for the computation, then when the electric field is applied, it becomes a superposition of the quasiground state and quasiexcited states of the full potential. The excited states are not bound so that they escape rapidly over the barrier. We attribute the initial surge to this and the oscillations in the surge to multiple reflections of these continuum states between the helium surface and the tunneling barrier.

[1] Gordon F. Saville, John M. Goodkind, and P. M. Platzman, Phys. Rev. Lett. **70**, 1517 (1993).

[2] Gordon F. Saville, Ph.D. thesis, University of California, San Diego, 1993.

[3] C. C. Grimes, T. R. Brown, Michael L. Burns, and C. L. Zipfel, Phys. Rev. B **13**, 140 (1976).

[4] S. Yücel and E. Y. Andrei, Phys. Rev. B **42**, 2088 (1990); Sermet Yücel and Eva Y. Andrei, *ibid.* **43**, 12 029 (1991).

[5] S. Geltman, J. Phys. B **11**, 3323 (1978).

[6] Abraham Goldberg, Harry M. Schey, and Judah L. Schwartz, Am. J. Phys. **35**, 177 (1967).

[7] Abraham Goldberg, Harry M. Schey, and Judah L. Schwartz, Am. J. Phys. **36**, 454 (1968).

[8] Ian Galbraith, Yin Sing Ching, and Eitan Abraham, Am. J. Phys. **52**, 60 (1984).

[9] C. Zipfel and T. M. Sanders, Jr., in *Proceedings of the Eleventh International Conference on Low Temperature Physics, 1968,* edited by J. F. Allen, D. M. Finlayson, and D. M. McCall (Organizing Committee of the Conference, St. Andrews, Scotland, 1969); W. Schoepe and G. W. Rayfield, Phys. Rev. A **7**, 2111 (1973); W. T. Sommer, Phys. Rev. Lett. **12**, 271 (1964).

[10] R. Price and P. M. Platzman, Phys. Rev. B **44**, 2356 (1992).

[11] Since the time constant for turning on the stripping field in the actual experiments was $t_c = 0.4$ msec, the measurements were made in the extreme adiabatic limit and there should be no initial transient surge. This was tested experimentally by comparing the amount of charge lost during a single long stripping pulse to that lost during a train of several shorter pulses. These measurements have shown no time dependence of the escape rate and the data limit the size of any tunneling surge in this adiabatic case to less than 5 parts in 10^6 per pulse, or approximately 200 times smaller than that appearing in the calculations for the sudden limit.

[12] M. Büttiker and R. Landauer, Phys. Rev. Lett. **49**, 1739 (1982); Phys. Scr. **32**, 429 (1985).

[13] L. E. Reichl, *The Transition to Chaos in Classical Systems: Quantum Manifestations* (Springer-Verlag, New York, 1992).

[14] *Quantum Chaos—Quantum Measurements,* edited by P. Cvitanovic, I. Percival, and A. Wirzba (Kluwer Academic, Dordrecht, 1992).

[15] K. Dietz, J. Henkel, and M. Holthaus, Phys. Rev. A **45**, 4960 (1992).

[16] E. J. Galvez, B. E. Sauer, L. Moorman, P. M. Koch, and D. Richards, Phys. Rev. Lett. **61**, 2011 (1988).

[17] R. Blümel, R. Graham, L. Sirko, U. Smilansky, H. Walther, and K. Yamada, Phys. Rev. Lett. **62**, 341 (1989).

[18] H. P. Breuer and M. Holthaus, J. Phys. (Paris) II **1**, 20 (1991).

[19] Roderick V. Jensen, Phys. Rev. A **30**, 386 (1984).

[20] Frank Grossman, Thomas Dittrich, Peter Jung, and Peter Hänggi, J. Stat. Phys. **70**, 229 (1993).

[21] Frank Grossman and Peter Hänggi, Chem. Phys. **170**, 295 (1993).

[22] Warren S. Warren, Herschel Rabitz, and Mohammed Dahleh, Science **259**, 1581 (1993).

[23] Y. Iye, K. Kono, K. Kajita, and W. Sasaki, J. Low Temp. Phys. **38**, 293 (1980).